Composites Science and Technology 199 (2020) 108360

Contents lists available at ScienceDirect

Composites Science and Technology

journal homepage: http://www.elsevier.com/locate/compscitech

# Pyrene-functionalized tetraphenylethylene polybenzoxazine for dispersing single-walled carbon nanotubes and energy storage

Maha Mohamed Samy [a], Mohamed Gamal Mohamed [a,b], Shiao-Wei Kuo [a,c,*]

[a] Department of Materials and Optoelectronic Science, Center of Crystal Research, National Sun Yat-Sen University, Kaohsiung, 80424, Taiwan
[b] Chemistry Department, Faculty of Science, Assiut University, Assiut, 71516, Egypt
[c] Department of Medicinal and Applied Chemistry, Kaohsiung Medical University, Kaohsiung, 807, Taiwan

ARTICLE INFO

*Keywords:*
Polybenzoxazine
Ring-opening polymerization
Carbon nanotube
Nanocomposites
Supercapacitor

ABSTRACT

We synthesized the new pyrene-functionalized tetraphenylethylene benzoxazine monomer (TPEP-BZ) through 1,1,2,2-tetra(3-formyl-4-hydroxyphenyl)ethylene with 1-aminopyrene through Schiff base reaction, reduction with $NaBH_4$ and then ring-closing with paraformaldehyde in a mixture of 1,4-dioxane and absolute EtOH. DSC, TGA, and FTIR spectroscopy were performed to understand the ring-opening polymerization and its corresponding thermal stability of this new TPEP-BZ monomer and then blending with different weight ratios of single-walled carbon nanotubes (SWCNT) before and after thermal treatments. More interestingly, the TPEP-BZ/SWCNT nanocomposites display lower curing temperature (262 °C), but significantly higher $T_d$ value (475 °C) and char yield (74 wt%) compared with typical Pa type benzoxazine. In addition, the poly (TPEP-BZ)/SWCNT nanocomposites also display high specific capacitance (84 F $g^{-1}$) at a current density of 0.5 A $g^{-1}$ and excellent cycling stability (98.3% capacitance retention over 2000 cycles).

## 1. Introduction

Polybenzoxazines (PBZs) are a class of new thermosetting resin, which has aroused scientific research interest and industrial attention [1–8]. The preparation of PBZs can be achieved through the thermal ring-opening polymerization of their benzoxazine rings, which is prepared from the Mannich condensation of aromatic phenols with the aromatic or aliphatic amine in the presence of formaldehyde or paraformaldehyde without using strong bases or acids and no releasing any side products [9–18]. They possess attractive characteristics compared to other typical thermosetting resins, like catalyst-free polymerization, high thermal stability, low flammability, flame retardance, high char yield, dimensional stability, low surface free energy, excellent mechanical and physical properties, flexible molecular design capability, low coefficient of thermal expansion, and low dielectric constant [19–24]. The improvement of thermal or mechanical properties of polybenzoxazines can be achieved through incorporation of nanofillers into benzoxazine matrix, such as clay, polyhedral oligomeric silsesquioxane, barium titanate nanoparticles, SiC whisker, and sol−gel nanoparticles into benzoxazine matrix, blending with different polymers (e.g. polyurethane, poly (N-vinyl-2-pyrrolidione), polyimide and epoxy resins) or copolymerization of benzoxazine with other monomers and introduction some functional groups including hydroxyl nitrile, allyl, phenylethynyl, ethynyl, propargyl, and alkyne group into benzoxazine monomers [25–33].

Carbon nanotubes (CNTs) have been also widely studied to create huge activity in the most areas of material science because of they have unique exceptional morphological structure, high stiffness, mechanical durability, electrical conductivity, chemical and physical properties and outstanding thermal conductivity due to the graphitic structure of nanotube lattice [34–41]. As reported in several literature reviews, all these unique properties make CNTs have a wide range of applications including field emission, conducting plastics, thermal conductors, conductive adhesives, thermal interface materials, catalyst supports, energy storage, fibers, ceramics, air and water filtrations [42,43]. Depending on the graphene layer number that presents in the CNT's wall, CNTs structure can be classified single-walled or multi-walled carbon nanotubes (SWCNT or MWCNT) [44,45]. They have already been successfully dispersed into benzoxazine matrices by two main approaches. The first one is covalent functionalization and the second one is non-covalent supramolecular adsorption of functional molecules onto CNT surfaces. The first one by the addition reactions of reagents to the

* Corresponding author. Department of Materials and Optoelectronic Science, Center of Crystal Research, National Sun Yat-Sen University, Kaohsiung, 80424, Taiwan.
*E-mail address:* kuosw@faculty.nsysu.edu.tw (S.-W. Kuo).

https://doi.org/10.1016/j.compscitech.2020.108360
Received 15 May 2020; Received in revised form 10 July 2020; Accepted 14 July 2020
Available online 21 July 2020

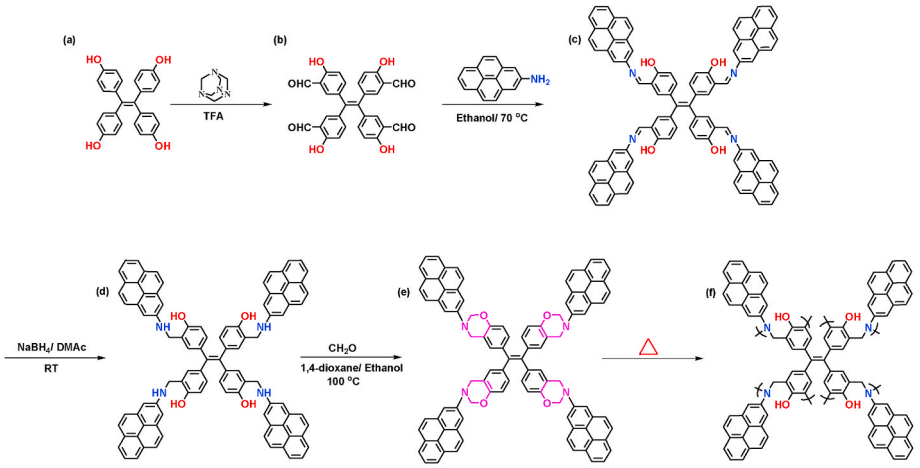


**Scheme 1.** Synthesis of (e) TPEP-BZ from (a) TPE-4OH, (b) TPE-4OH–CHO, (c) TPEP Schiff base, (d) TPEP-hydroxybenzylamine, and to form (f) poly (TPEP-BZ) after thermal curing.

sidewalls or by modifying the CNT surfaces with molecules or reactive groups such as OH, COOH to promote their dispersion in solvents or polymer matrices [46–50]. Furthermore, Chen et al. proposed that the curing temperature of benzoxazine monomers decreased and the ring-opening process catalyzed due to the surface carboxyl units of CNTs [36]. The limitations of this approach are the disruption of graphitic skeleton and loss of electronic properties. The noncovalent approach is a method for tuning the interfacial properties of CNTs. The difference between this method and the covalent one involves π-π stacking interactions between the CNT surface and the polymer chains [36–39]. Also, the noncovalent approach of CNTs does not change the nanotubes structure and electronic network, which can enhance dispersibility, thus, the physical properties of CNTs should retain unaffected [34,37,39]. Indeed, the preparation and fabrication polymers with these nanofillers [CNTs] can be used in many potential applications such as energy storage and nanoelectronic [34,39,51]. CNTs are considered as amazing materials in energy storage applications and widely used in the electrode fabrication for supercapacitors (SCs) and lithium batteries (LIBs) as a supporter and an active material due to their excellent electrical conductivity, higher ion accessibility and interesting unique morphology compared to other conductive additives such as graphite, carbon black and carbon nanofibers. Some groups found that the power density of both supercapacitors (SCs) and lithium batteries (LIBs) significantly enhanced and improved after incorporation CNTs into the electrodes of LIBs and SCs [52,53]. According to Dumas et al. result, the π-π stacking interaction between p-phenylenediamine benzoxazine and CNTs led to form the reinforced network with excellent mechanical and thermal properties of PBZ structure and enhanced the dispersion of the CNTs in PBZ matrix [54]. We found that the bifunctional (Coumarin-Py BZ) monomer with pyrene and coumarin moieties could be improved the SWCNT dispersion inside the polybenzoxazine matrix by π-π stacking between SWCNT and pyrene units, and formation of nanohybrids. Furthermore, these composites exhibiting high char yield and glass transition temperature of the polybenzoxazine matrix after

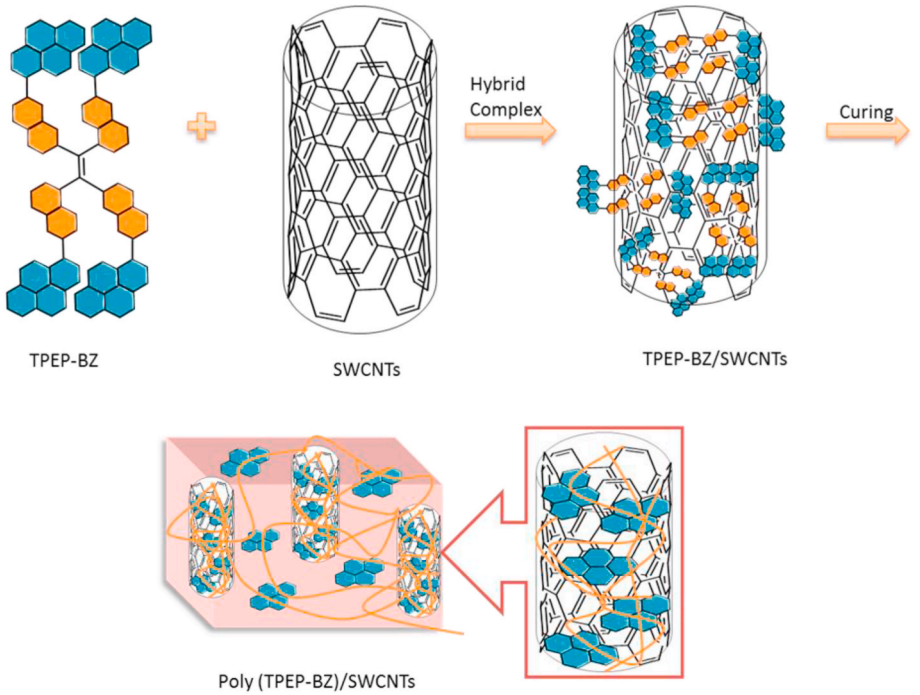


**Scheme 2.** The formation of TPEP-BZ/SWCNT hybrid complex to form poly (TPEP-BZ)/SWCNT nanocomposites after thermal treatment.

photo-dimerization of coumarin units through [2π + 2π] cycloaddition [55]. In addition, we also synthesized multifunctional (Azo–COOH–Py BZ) benzoxazine monomer possessing the azobenzene unit, pyrene moiety, and carboxylic acid group. We revealed that when the content of SWCNTs (5 wt%), the exothermic curing peak of Azo–COOH–Py BZ (226 °C) was lowered to (194 °C), which indicated that CNTs worked as initiator and catalysts for the ring-opening polymerization of oxazine unit [56]. Liu et al. prepared PBz-MWCNT using both a thermally activated radical and addition reactions [24]. They found that these materials showed good homogeneous dispersion inside PBZ matrix, high interfacial compatibility, and anticorrosion property compared with that the neat crosslinked PBz. Also, Dumas et al. prepared P-pPDA/CF laminate composites with 0.5 wt% of CNTs and they revealed that these composites possess excellent thermomechanical stability (above 300 °C), flexural strength (700 MPa), flexural modulus (59 Gpa) and fire resistance improved significantly [57].

Based on those previous results, the functionality of pyrene into the benzoxazine monomer is usually a mono-functional unit [54–56]. To improve the π-π stacking between SWCNT and pyrene units, in this report, we have been successfully prepared a tetra-functionalized benzoxazine monomer (TPEP-BZ) containing tetraphenylethylene and pyrene units. The reaction of 1,1,2,2-Tetra (3-formyl-4-hydroxyphenyl) ethylene (TPE-4OH–CHO, Scheme 1(a)) with 1-aminopyrene in absolute EtOH to form TPEP Schiff base compound (Scheme 1(b)). The reaction of TPEP hydroxybenzylamine (Scheme 1(c)) from the reduction of TPEP Schiff base with paraformaldehyde in a mixture of 1,4-dioxane and absolute EtOH could form TPEP-BZ (Scheme 1(d)). Then, we blended TPEP-BZ monomer with different amounts of SWCNT to form stable poly (TPEP-BZ)/SWCNT nanocomposites through strong π–π interactions between SWCNT and pyrene unit in TPEP-BZ, as depicted in Scheme 2. Thermogravimetric analysis (TGA), Fourier transform infrared (FTIR) spectroscopy, and differential scanning calorimetry (DSC) were performed to examine the thermal stability and thermal curing behavior of TPEP-BZ in the presence and absence of SWCNT. In addition, the dispersion SWCNT in the TPEP-BZ matrix after thermal curing was confirmed by using transmission electron microscopy (TEM) and photoluminescence spectroscopy. The electrochemical analyses were done to investigate the potential application of poly (TPEP-BZ)/SWCNT nanocomposites as electrode materials for energy storage performance. To the best of our knowledge, this is the first report to study and present the electrochemical performance of poly (TPEP-BZ)/SWCNTs nanocomposites based on tetraphenylethylene and pyrene units.

## 2. Experimental

### 2.1. Materials

4,4′-Dihydroxybenzophenone, dimethylacetamide (DMAc), MeOH, absolute EtOH (99.99%), tetrahydrofuran (THF), aniline, zinc powder, potassium carbonate ($K_2CO_3$), titanium tetrachloride ($TiCl_4$), sodium borohydride ($NaBH_4$), hexamethylenetetramine, sodium bicarbonate ($NaHCO_3$) and trifluoroacetic acid (TFA) were purchased from Sigma–Aldrich. Paraformaldehyde, 1,4-dioxane and acetone were purchased from Acros. SWCNTs were obtained from Center Biochemistry Technology. Tetra (*p*-hydroxyphenyl)ethylene (TPE-4OH), (1,1,2,2-tetra(3-formyl-4-hydroxyphenyl)ethylene) (TPE-4OH–CHO) and 1-aminopyrene (Py-$NH_2$), were synthesized using the previously reported procedures [58–61].

### 2.2. 4,4'-((1Z)-1,2-bis(4-hydroxy-3-((pyren-1-ylimino)methyl)phenyl) ethene-1,2diyl)bis(2-((pyren-4-ylimino)methyl)phenol) (TPEP schiff base)

TPE-4OH–CHO (0.70 g, 1.37 mmol) and 1-aminopyrene (1.19 g, 5.47 mmol) in absolute EtOH (50 mL) were refluxed at 70 °C for 24 h. The yellow product formed was filtered off, washed several times with MeOH and finally dried to give the powder (1.20 g, 70%). FT-IR (KBr, $cm^{-1}$): 3448 (OH), 3038 (aromatic C–H), 1620 (C═N). $^1H$ and $^{13}C$ NMR analyses are not done because of its poor solubility.

### 2.3. (Z)-4,4'-(1,2-bis(4-hydroxy-3-((pyren-1-ylamino)methyl)phenyl) ethene-1,2-diyl)bis(2-((pyren-4-ylamino)methyl)phenol) (TPEP hydroxybenzylamine)

$NaBH_4$ (0.09 g, 2.37 mmol) and TPEP Schiff base (0.55 g, 0.42 mmol) were dissolved in DMAc (10 mL) and the solution mixture was stirred at 25 °C for 1 day. Then, the solution mixture was poured onto 500 mL of cold water to afford a black powder (0.45 g, 82%). FTIR (KBr, $cm^{-1}$): 3410 (O–H), 3326 (N–H). $^1H$ NMR (500 MHz, DMSO-$d_6$, δ (ppm)): 9.45 (OH), 9.15 (NH), 8.31–6.56 (ArH), 4.17 ($NCH_2$). $^{13}C$ NMR (125 MHz, DMSO-$d_6$, $\delta$ (ppm)): 154.14, 145.07, 143.36, 138.56, 135.79, 132.02, 132.04, 131.45, 130.629, 127.73, 127.35, 126.55, 125.91, 125.26, 125.08, 124.15, 123.00, 122.94, 122.15, 121.77, 121.14, 115.36, 42.55. FTMS: calcd. for $C_{94}H_{64}N_4O_4$, *m/z* 1312.49; found 1311.48 (Fig. S1).

### 2.4. 1, 1, 2, 2-tetrakis(3-(pyren-1-yl)-3,4-dihydro-2H-benzo[e][1,3] oxazin-6-yl)ethane (TPEP-BZ)

In a 250 mL two-neck flask, TPEP hydroxybenzylamine (0.45 g, 0.34 mmol) and paraformaldehyde (0.05 g, 16.66 mmol) were dissolved in a mixture of absolute EtOH and 1, 4-dioxane (60 mL). After that, the solution mixture was heated at 90 °C for 1 day and then we evaporated the solvents. The brown residue was extracted three times by EtOAc (100 mL) and aqueous $NaHCO_3$ (1 wt%, 100 mL). After that, the EtOAc solution was dried over anhydrous $MgSO_4$ and evaporated under pressure to give a yellow solid (0.40 g, 87%). FTIR (KBr, $cm^{-1}$): 1236 (asymmetric C–O–C stretching), 1027 (symmetric C–O–C stretching), 934 (vibration of the oxazine ring). $^1H$ NMR $^1H$ NMR (500 MHz, DMSO-$d_6$, δ (ppm)): 8.28–6.61 (ArH), 5.19 (s, $OCH_2N$), 4.37 (s, $NCH_2Ar$). $^{13}C$ NMR (125 MHz, DMSO-$d_6$, δ (ppm)): 152.83, 143.52, 138.92, 136.80, 131.80, 129.88, 127.78, 127.32, 126.98, 126.29, 125.79, 125.12, 125.05, 124.89, 124.62, 123.62, 122.48, 120.10, 119.13, 115.64, 82.00 ($OCH_2N$), 51.62 (Ar- $CH_2N$). FTMS: calcd. for $C_{98}H_{64}N_4O_4$, *m/z* 1361.61; found 1361.49 (Fig. S2).

### 2.5. Poly(TPEP-BZ)/SWCNTs nanocomposites

TPEP-BZ monomer with different amounts of SWCNT were both dissolved in THF. Then, the THF solution was stirred at room temperature for 8 h and then the THF was evaporated at 50 °C for 24 h in the oven. Each sample was thermally cured at 110, 150, 180, 210 and 250 °C for 2 h at each temperature to form pure poly (TPEP-BZ), poly (TPEP-BZ)/SWCNT-1 (1 wt% SWCNT) and poly (TPEP-BZ)/SWCNT-5 (5 wt% SWCNT) nanocomposites [Scheme 2].

## 3. Results and discussion

### 3.1. Synthesis of TPEP-BZ monomer

In this study, we prepared TPEP-BZ monomer through the three-step procedure. First, from the condensation reaction of TPE-4OH–CHO with Py-$NH_2$ in absolute ethanol. Next, TPEP hydroxybenzylamine was synthesized through $NaBH_4$-mediated reduction of the TPEP Schiff base. Finally, we obtained the TPEP-BZ monomer through a ring-closing between TPEP hydroxybenzylamine and paraformaldehyde in a mixture of 1, 4-dioxane and EtOH at 100 °C (Scheme 1). Fig. 1 displays $^1H$ and $^{13}C$ NMR spectra of TPEP hydroxybenzylamine, and TPEP-BZ monomer, respectively. The $^1H$ spectrum of TPEP hydroxybenzylamine [Fig. 1(a)] features the proton signals at 4.17, 9.15, and 9.45 ppm corresponding to its N–**$CH_2$**, OH, and NH groups, respectively. The oxazine ring of TPEP-BZ [Fig. 1(b)] was featured by two signals at 4.37 (Ar-**$CH_2$**N) and 5.19 (O**$CH_2$**N) ppm, indicating the successful preparation of TPEP-BZ

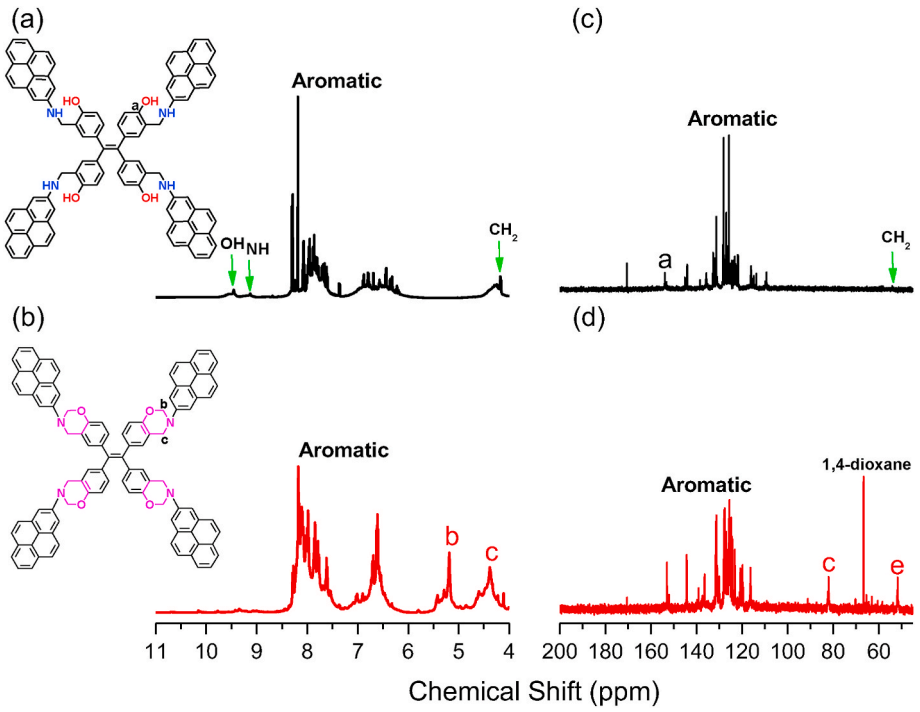


**Fig. 1.** $^{1}H$ and $^{13}C$ NMR spectra of TPEP hydroxybenzylamine (a, c) and TPEP-BZ monomer (b, d) at room temperature.

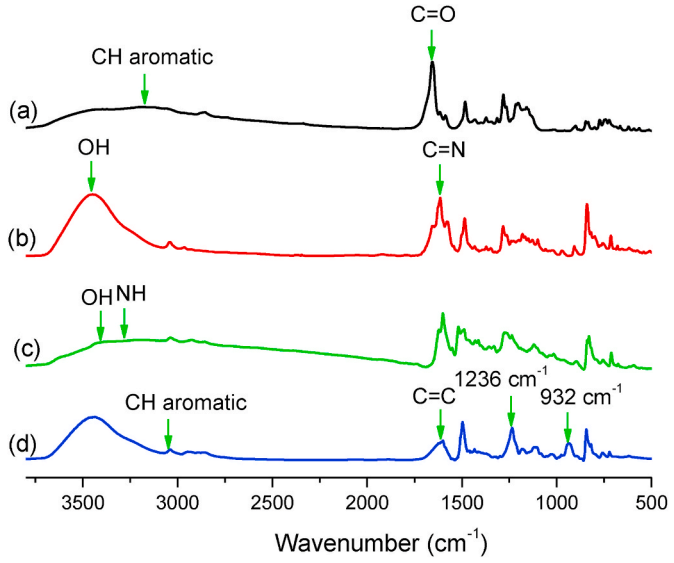


**Fig. 2.** FTIR spectra of (a) TPE-4OH–CHO, (b) TPEP Schiff base, (c) TPEP hydroxybenzylamine, and (d) TPEP-BZ monomer at room temperature.

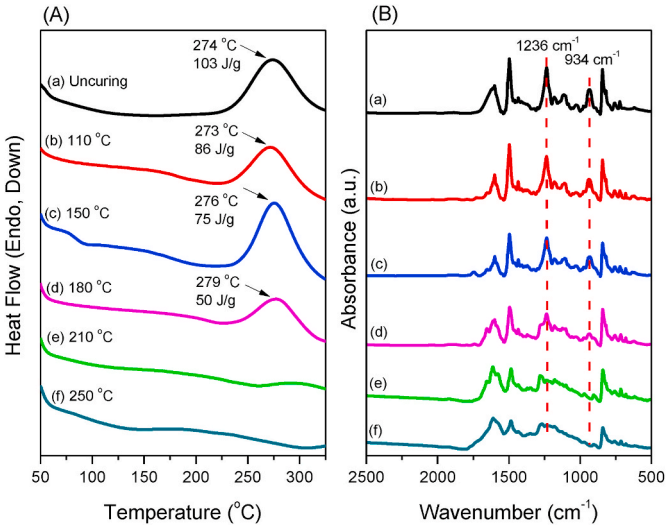


**Fig. 3.** (A) DSC and (B) FTIR analyses of TPEP-BZ after curing at various temperatures.

monomer [62–66]. Fig. 1(c) and (d) represent $^{13}C$ NMR spectra of TPEP hydroxybenzylamine and TPEP-BZ monomer in DMSO-$d_6$. The characteristic carbon signals for the NH**CH$_2$** and aromatic carbon attached to OH in TPEP hydroxybenzylamine centered at 42.55 and 153.59 ppm, respectively [Fig. 1(c)]. In the profile of TPEP-BZ monomer [Fig. 1(d)], the characteristic signals of TPEP-BZ appeared at 51.62 and 82.00 ppm for the Ar-**C**H$_2$N and O**C**H$_2$N units [62–66].

Fig. 2 presents the FTIR spectra of TPE-4OH–CHO, TPEP Schiff base, TPEP hydroxybenzylamine, and TPEP-BZ. The spectrum of TPE-4OH–CHO features absorption band at 1650 cm$^{-1}$ for the C=O unit and characteristics absorptions bands for aliphatic C–H stretching of the CHO group at 2859 and 2740 cm$^{-1}$ [Fig. 2(a)]. While the FTIR profile of the TPEP Schiff base shows a broad peak for OH group at 3448 cm$^{-1}$ and a sharp peak for C=N stretching appears at 1620 cm$^{-1}$ [Fig. 2(b)]. After reduction of the TPEP Schiff base, we observed the characteristic absorption peaks of the TPEP hydroxybenzylamine [Fig. 2(c)] appeared at 2929, 3326 and 3410 cm$^{-1}$ for C–H aliphatic groups, N–H and phenolic O–H, respectively, indicative the complete reduction of the TPEP Schiff base. In the spectrum of TPEP-BZ monomer [Fig. 2(d)], the absorption bands for the OH and NH groups completely disappeared and there is new characteristic absorption bands of a benzoxazine structure for stretching vibrations of oxazine ring (934 cm$^{-1}$), symmetric C–O–C stretching (1027 cm$^{-1}$), and asymmetric C–O–C stretching (1236 cm$^{-1}$). Also, the spectrum of TPEP-BZ monomer displayed the characteristic absorption bands at 3032 and 1614 cm$^{-1}$ for its aromatic rings and C=C stretching. Furthermore, we recorded FT mass spectra to confirm the chemical structure and synthesis of the TPEP hydroxybenzylamine and

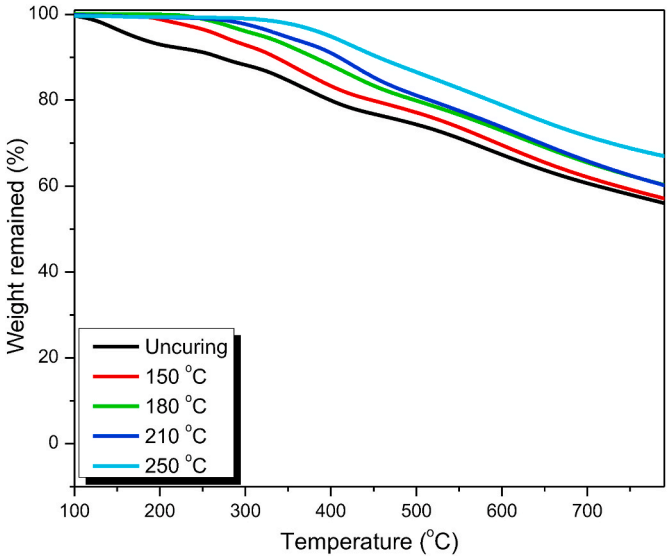


**Fig. 4.** TGA analyses of TPEP-BZ monomer determined after each curing temperature.

TPEP-BZ monomer. Figs. S1 and S2 display that the molecular weights of the TPEP hydroxybenzylamine and TPEP-BZ monomer were *m/z* of 1311.48 and 1361.48, which are consistent with their calculated values (*m/z* of 1312.49 and 1361.61 respectively). From the data above results, NMR, FTIR, and mass spectroscopic results were confirmed the successful synthesis of TPEP-BZ monomer in this study.

### 3.2. Thermal polymerization of TPEP-BZ monomer

DSC and FTIR analyses were used to investigate the thermal ring-opening polymerization of the TPEP-BZ monomer. Fig. 3(A) represents the DSC profile of TPEP-BZ after each curing temperature. As shown in Fig. 3 (A), the uncured TPEP-BZ monomer reveals a curing temperature of 274 °C with a reaction heat of 103 J/g. The exothermic curing temperature of uncured TPEP-BZ monomer from an amino-pyrene unit is higher than TPE-BZ from aniline unit (250 °C), indicating that the bulk pyrene unit is difficult to ring-opening the oxazine ring as expected. However, this value is lower than that (286 °C) of pyrene-functionalized benzoxazine (Py–BZ) without the TPE unit [61]. Interestingly, our new TPEP-BZ monomer (274 °C) exhibited the similar exothermic curing temperature like furan with tetrafunctional fluorene benzoxazine (t-BF-f, 279 °C) and the cardanol with tetrafunctional fluorene benzoxazine m (t-BF-a-c, 276 °C) [67,68]. After thermal treatment of the TPEP-BZ at 110, 150, 180 and 210 °C, the exothermic curing temperature peak of TPEP-BZ decreased and disappeared totally after thermal curing temperature at 250 °C, suggesting that the ring-opening polymerization of TPEP-BZ was completed at 250 °C. Fig. 3(B) represents FTIR spectra of TPEP-BZ after each curing step (from 110 to 250 °C), to investigate its polymerization behavior. The intensities of the absorption bands of the BZ structure at 1236 (asymmetric COC stretching) and 934 $cm^{-1}$ (oxazine ring) gradually decreased and disappeared completely with raising the curing temperature.

Based on TGA analysis [Fig. 4 and Table S1], the thermal decomposition temperature ($T_{d5}$ or $T_{d10}$), and weight residue at 800 °C (char

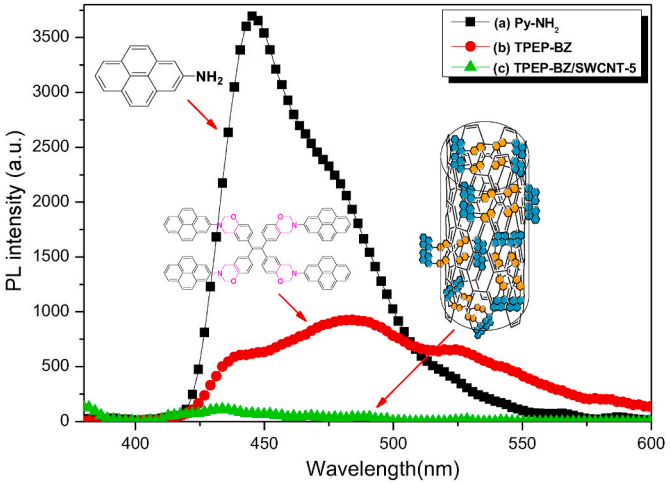


**Fig. 6.** PL spectra of (a) Py-$NH_2$, (b)TPEP-BZ, monomer and (c) TPEP-BZ/SWCNT-5 in THF solution ($\lambda_{ex}$ = 365 nm).

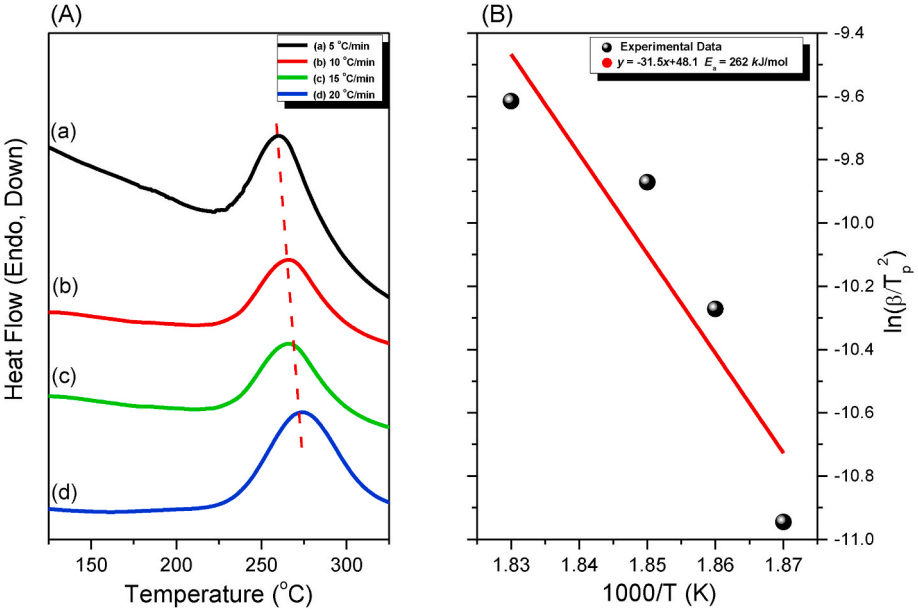


**Fig. 5.** (A) Dynamic DSC exothermic curve for TPEP-BZ monomer, recorded at various heating rates, (B) Kissinger plots, for the determination of the value of $E_a$, of TPEP-BZ.

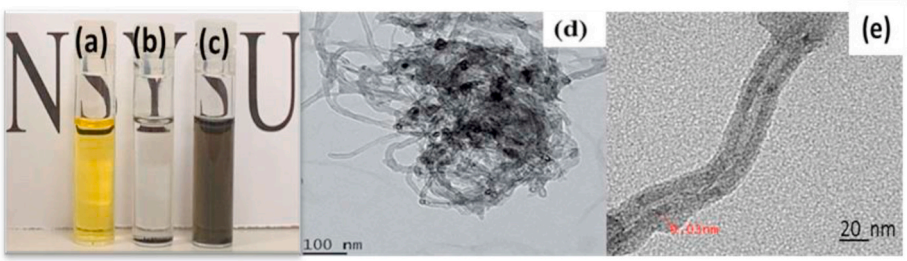


**Fig. 7.** Photographs of (a) TPEP-BZ, (b) SWCNT, and (c) TPEP-BZ/SWCNTs hybrid complex in THF. TEM images of (d) pure SWCNT and (e) poly (TPEP-BZ)/SWCNT-5 after thermal curing at 250 °C.

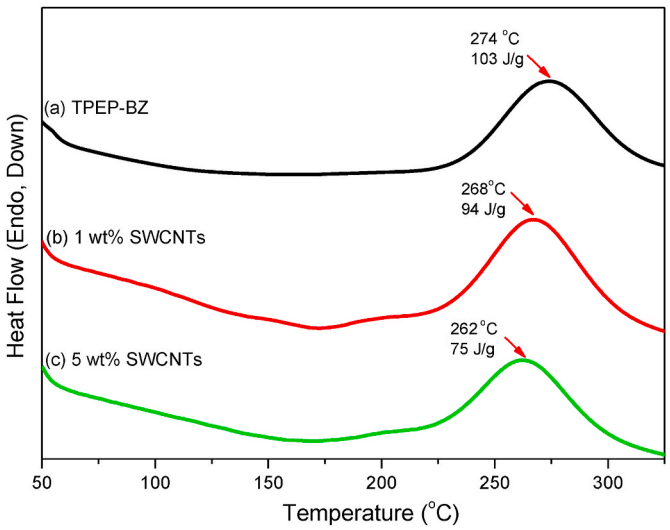


**Fig. 8.** DSC analyses of (a) TPEP-BZ, (b) TPEP-BZ/SWCNT-1, and (c) TPEP-BZ/SWCNT-5 hybrid complex before thermal curing.

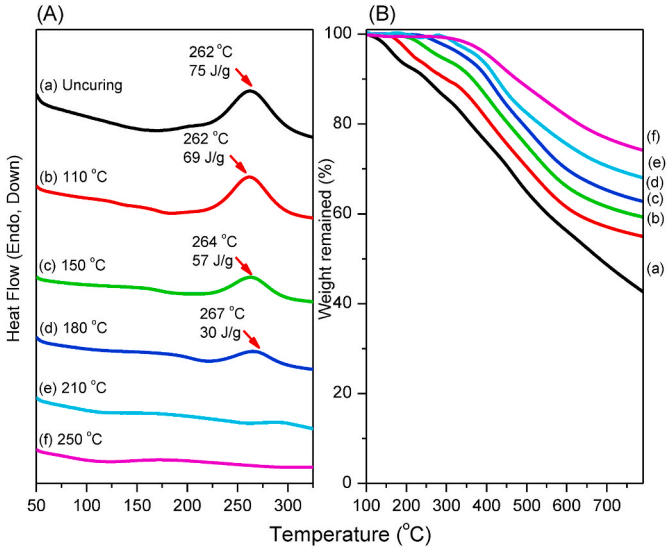


**Fig. 9.** (A) DSC and (B) TGA analyses of TPEP-BZ/SWCNT-5 before and after thermal curing.

yield) of the poly (TPEP-BZ) were increased upon increasing the curing temperature, probably due to the increase of crosslinking density after thermal curing of the TPEP-BZ monomer. In addition, we found that after thermal treatment at 250 °C, the ($T_{d5}$, $_{d10}$) and the char yield increased significantly to 398, 455 °C and 67 wt%, respectively. When

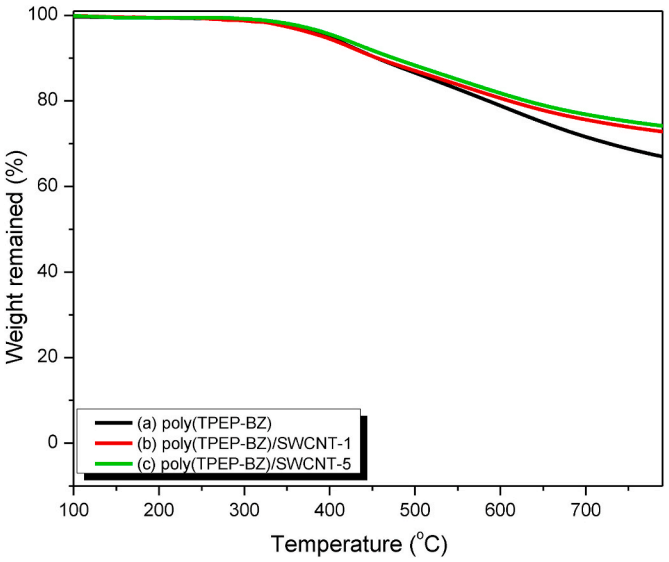


**Fig. 10.** TGA analyses of (a) poly (TPEP-BZ), (b) poly (TPEP-BZ)/SWCNT-1, and (c) poly (TPEP-BZ)/SWCNT-5 hybrid complexes after thermal curing at 250 °C.

compared with the thermal stability of typical model Pa-BZ, Py-BZ, and TPE-BZ, their char yield was only 43, 26 and 64 wt%, thus our new poly (TPEP-BZ) displayed much higher value than those of the model benzoxazines [60,61,68].

Furthermore, the curing kinetics of the TPEP-BZ monomer was investigated by using the Kissinger method. In this method, the activation energy (*Ea*) of the TPEP-BZ monomer could be calculated according to equation (1) [69]:

$$\ln\left(\frac{\beta}{T_p^2}\right) = \ln\left(\frac{AR}{E_a}\right) - \frac{E_a}{RT} \quad (1)$$

where $A$ is the frequency factor; $\beta$ is the constant heating rate, $R$ is the gas constant, and $T_p$ is the exothermic curing peak. From Fig. 5(A), we observed that the curing peak was increased upon increasing heating rate due to the delay thermal curing reaction. Based on Fig. 5(B), we found that the calculated activation energy for the polymerization reaction of TPEP-BZ was 262 kJ mol$^{-1}$, which is higher than TPE-BZ monomer (141 kJ mol$^{-1}$) [60], also indicating that the bulk pyrene unit is difficult to ring-opening the oxazine ring.

### 3.3. Thermal behavior of TPEP-BZ/SWCNT nanocomposites

Fig. 6 exhibits the PL spectra of Py–$NH_2$, TPEP-BZ, and TPEP-BZ/SWCNT-5 in THF solution at the excitation wavelength (365 nm). From PL spectra we observed a fluorescence signal due to pyrene unit of Py–$NH_2$ and a broad signal due to of TPEP-BZ but we observed a very

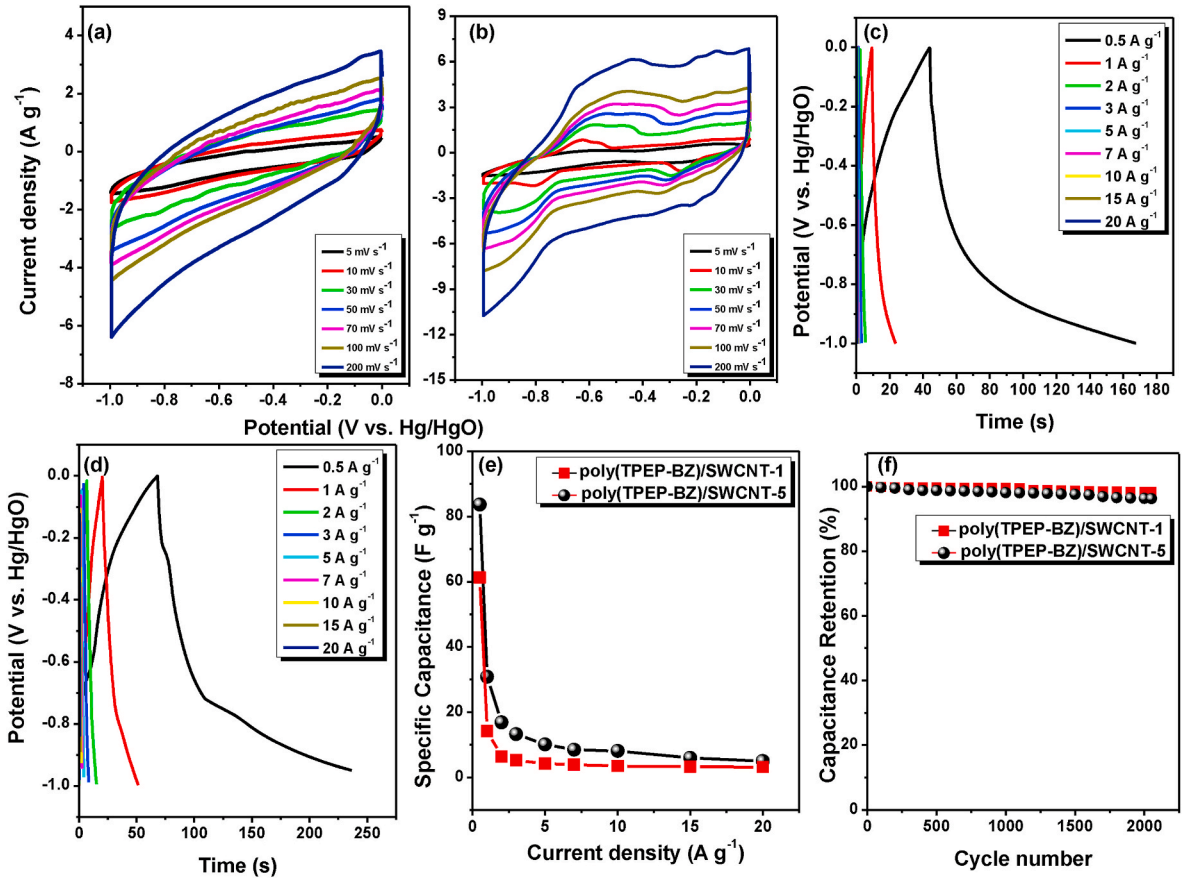


**Fig. 11.** CV curves of (a) poly (TPEP-BZ)/SWCNT-1 and (b) poly (TPEP-BZ)/SWCNT-5. (c, d) GCD curves of (c) poly (TPEP-BZ)/SWCNT-1 and (d) poly (TPEP-BZ)/SWCNT-5, recorded at various currents. (e) Specific capacitance of poly (TPEP-BZ)/SWCNT-1 and poly (TPEP-BZ)/SWCNT-5, recorded at current densities from 0.5 to 20 A/g. (f) Cycling stabilities of poly (TPEP-BZ)/SWCNT-1 and poly (TPEP-BZ)/SWCNT-5, electrodes, recorded at current density of 10 A/g over 2000 cycle.

weak emission of TPEP-BZ/SWCNT-5 and the quenched fluorescence of pyrene unit completely, indicating the presence of strong π–π stacking interactions between the TPEP-BZ monomer and SWCNT and occurrence energy transfer between the light-emitted pyrene unit and the SWCNTs [55,56,61].

Fig. 7(a–e) represent photographs of pure TPEP-BZ monomer, pure SWCNT, and the TPEP-BZ/SWCNT hybrid nanocomposite in THF solutions, respectively. The TPEP-BZ displayed clear solution (Fig. 7(a)), while the SWCNT formed a precipitate (Fig. 7(b)), which as confirmed in TEM image [Fig. 7(d)], but the addition of TPEP-BZ in SWCNTs suspension lead to a dispersion [Fig. 7(c)], suggesting that dissolving complexes formed due to noncovalent interactions (π-π stacking), then we examined the dispersion of SWCNT (5 wt %) in the TPEP-BZ monomer by TEM (Fig. 7(e)) exhibits the uniform dispersion of SWCNT within the TPEP-BZ matrix.

By DSC profile we investigated the thermal curing behavior of TPEP-BZ monomer using different weight percentages of SWCNT, as displayed in Fig. 8. We observed that the addition of SWCNT was decreased the thermal curing peak of TPEP-BZ. The curing temperature of the exotherm peak for TPEP-BZ shifted from 274 to 268 and 262 °C after blending with 1 and 5 wt% of SWCNT, respectively. According to previous studies [70,71], this decrease in the curing temperatures after blending with CNTs attributable to it could act as the catalyst for initiating the opening of the benzoxazine ring.

We also investigated the curing behavior and thermal stabilities of TPEP-BZ/SWCNT-5 hybrid complexes before and after thermal treatments as shown in Fig. 9. Based on DSC analysis [Fig. 9(A)], we found that the maximum exotherm curing peak decreased with raising the curing temperature as noted above until reaching zero at the curing temperature of 250 °C. Also, the exotherm curing peak of the TPEP-BZ/SWCNT-5 was increased by increasing the curing temperature. TGA thermograms [Fig. 9(B)], showed the decomposition temperatures ($T_{d10}$) of the TPEP-BZ/SWCNT-5 were 250, 300, 365, 404, 426 and 475 °C after thermal treatments at 25, 110, 150, 180, 210 and 250 °C. We also check DMA analysis of poly (TPEP-BZ) and poly (TPEP-BZ)/SWCNT-1, after thermal treatment at 250 °C for 2 h, as presented in Fig. S3. As shown in Fig. S3, the $T_g$ values of poly (TPE-BZ) and poly (TPEP-BZ)/SWCNT-1 were observed both at ca. 279 °C. As expected, the $T_g$ value of poly (TPEP-BZ) does not seem to be affected after the addition of the SWCNTs into the TPEP-BZ matrix [55,61,72].

Fig. 10 showed the TGA profile of the poly (TPEP-BZ)/SWCNT nanocomposites after thermal curing at 250 °C under a $N_2$ atmosphere. The values of the decomposition temperatures ($T_{d10}$) of poly (TPEP-BZ)/SWCNT-1 (456 °C) and poly (TPEP-BZ)/SWCNT-5 (475 °C) were higher than the pure poly (TPEP-BZ) (455 °C). Furthermore, the weight residue of poly (TPEP-BZ) was increased upon increasing of the SWCNT contents. This is due to the introduction of SWCNTs into the PBZ matrix would block the premature evaporation from the decomposed molecular fragments and leads to the network structure formation after incorporating inorganic CNTs [55,56,61]. More interestingly, the TPEP-BZ/SWCNT-5 displays lower curing temperature (262 °C) compared with the typical model Pa-BZ monomer (263 °C); however, it displays significantly higher $T_d$ value (475 °C vs. 391 °C) and char yield (74 wt% vs. 43 wt%). Furthermore, our thermally cured poly (TPEP-BZ)/SWCNT-5 displays the highest thermal stability compared with any other reported PBZ with a CNT system based on our knowledge as shown in Table S2.

### 3.4. Electrochemical performance

To investigate the electrochemical performance of the poly (TPEP-BZ)/SWCNT nanocomposites, we measured cyclic voltammetry (CV) with different scan rates of the assembled supercapacitor (5–200 mV $s^{-1}$) in 1 M aqueous KOH [Fig. 11(a) and (b)]. As seen in Fig. 11(a) and (b), the poly (TPEP-BZ)/SWCNT-1 and poly (TPEP-BZ)/SWCNT-5 had a quasi-rectangular voltammogram shape with the redox peaks [73–75], suggesting that the combination of electric double-layer capacitance and pseudocapacitance characteristics. Fig. 11(c) and (d) display the galvanostatic charge/discharge (GCD) profiles of the poly (TPEP-BZ)/SWCNT-1 and poly (TPEP-BZ)/SWCNT-5 recorded at various current density ranges from 0.5 to 20 A/g. The shape of the GCD curves of both two PBZ nanocomposites materials had triangular shapes, which also suggested that the main energy storage mechanism of the electrode was EDLC and pseudocapacitance. Furthermore, the poly (TPEP-BZ)/SWCNT-5 had a longer discharge time than that of poly (TPEP-BZ)/SWCNT-1 at all current densities, which indicated that the poly (TPEP-BZ)/SWCNT-5 was suitable for rapid charge-discharge operation as an electrode material. Notably, the poly (TPEP-BZ)/SWCNT-5 electrode [Fig. 11 (e)] exhibits the highest specific capacitance value (84 F $g^{-1}$) compared to the poly (TPEP-BZ)/SWCNT-1 (61 F $g^{-1}$) at the current density of 0.5 A/g, which presumably arising from the higher content of SWCNTs in poly (TPEP-BZ)/SWCNT (5 wt%). Fig. 11(f) shows the cycling stability of the poly (TPEP-BZ)/SWCNT-1 and the poly (TPEP-BZ)/SWCNT-5 electrodes at the current density of 10 A/g. After 2000 cycles of charge and discharge, the capacitance retention rate values were 96.30% and 98.33% for poly (TPEP-BZ)/SWCNT-1 and poly (TPEP-BZ)/SWCNT-5, respectively, suggested that these materials had excellent cycling stability and were suitable for use in supercapacitors application. Thus, the combination of TPEP-BZ with SWCNTs nanocomposites could be opened and offers an attractive route to enhance the performance of the electrode.

## 4. Conclusions

We have synthesized the tetrafunctional benzoxazine monomer (TPEP-BZ) containing tetraphenylethylene and pyrene groups that enhance the dispersity of SWCNTs in THF solution and lead to the formation of highly soluble TPEP-BZ/SWCNT organic/inorganic nanocomposites. From DSC and TGA analyses, we found that after blending TPEP-BZ with various content of SWCNTs, the exothermic curing peak is decreased; confirming that the addition of the SWCNTs into the TPEP-BZ matrix can catalyze the thermal curing process and also display excellent thermal properties of poly (TPEP-BZ) compared with other PBZ systems. More interestingly, the electrochemical performances of poly (TPEP-BZ)/SWCNT-5 was highly stable and efficient, with the capacitance of 84 F $g^{-1}$ at 0.5 mV $s^{-1}$ and long-term cycling stability of 98.33% capacitance retention rate after 2000 cycle. Finally, the combination of PBZ with SWCNTs nanocomposites could be acted as the promising alternative route for the high-performance electrode materials in energy storage applications.

## Declaration of competing interest

The authors declare that they have no known competing financial interests or personal relationships that could have appeared to influence the work reported in this paper.

## CRediT authorship contribution statement

**Maha Mohamed Samy:** Data curation, Writing - original draft. **Mohamed Gamal Mohamed:** Data curation, Writing - original draft. **Shiao-Wei Kuo:** Supervision, Writing - review & editing.

## Acknowledgments

This study was supported financially by the Ministry of Science and Technology, Taiwan, under contracts MOST 106-2221-E-110- 067-MY3, 108-2638-E-002-003-MY2, and 108-2221-E-110-014-MY3.

## Appendix A. Supplementary data

Supplementary data to this article can be found online at https://doi.org/10.1016/j.compscitech.2020.108360.

## References

[1] X. Ning, H. Ishida, Phenolic materials via ring-opening polymerization: synthesis and characterization of bisphenol-A based benzoxazines and their polymers, J. Polym. Sci., Part A: Polym. Chem. 32 (1994) 1121–1129.
[2] N.N. Ghosh, B. Kiskan, Y. Yagci, Polybenzoxazines of new high-performance thermosetting resins: synthesis and properties, Prog. Polym. Sci. 32 (2007) 1344–1391.
[3] L. Han, M.L. Salum, K. Zhang, P. Froimowicz, H. Ishida, Intrinsic self-initiating thermal ring-opening polymerization of 1, 3- benzoxazines without the influence of impurities using very high purity crystals, J. Polym. Sci., Part A: Polym. Chem. 55 (2017) 3434–3445.
[4] S. Ohashi, D. Iguchi, T.R. Heyl, P. Froimowicz, H. Ishida, Quantitative studies on the p-substituent effect of the phenolic component on the polymerization of benzoxazines, Polym. Chem. 9 (2018) 4194–4204.
[5] K. Zhang, X.X. Tan, Y.T. Wang, H. Ishida, Unique self-catalyzed cationic ring-opening polymerization of a high performance deoxybenzoin-based 1,3-benzoxazine monomer, Polymer 168 (2019) 8–15.
[6] K.I. Aly, M.G. Mohamed, O. Younis, M.H. Mahross, M.A. Hakim, M.M. Sayed, Salicylaldehyde azine-functionalized polybenzoxazine: synthesis, characterization, and its nanocomposites as coatings for inhibiting the mild steel corrosion, Prog. Org. Coating 138 (2020) 105385.
[7] K. Zhang, M.C. Han, L. Han, H. Ishida, Resveratrol-based tri-functional benzoxazines: synthesis, characterization, polymerization, and thermal and flame retardant properties, Eur. Polym. J. 116 (2019) 526–533.
[8] M.G. Mohamed, S.W. Kuo, Polybenzoxazine/polyhedral oligomeric silsesquioxane (POSS) nanocomposites, Polymers 8 (2016) 225.
[9] M.G. Mohamed, S.W. Kuo, Functional silica and carbon nanocomposites based on polybenzoxazines, Macromol. Chem. Phys. 220 (2019) 1800306.
[10] F. Shan, S. Ohashi, A. Erlichman, H. Ishida, Non-flammable thiazole functional monobenzoxazines: synthesis, polymerization, thermal and thermomechanical properties, and flammability studies, Polymer 157 (2018) 38–49.
[11] J. Liu, N. Safronava, R.E. Lyon, J. Maia, H. Ishida, Enhanced thermal property and flame retardancy via intramolecular 5- membered ring hydrogen bond-forming amide functional benzoxazine resins, Macromolecules 51 (2018) 9982–9991.
[12] K. Zhang, H. Ishida, An anomalous trade-off effect on the properties of smart ortho-functional benzoxazines, Polym. Chem. 6 (2015) 2541–2550.
[13] S.W. Kuo, Y.C. Wu, C.F. Wang, K.U. Jeong, Preparing Low-surface-energy polymer materials by minimizing intermolecular hydrogen-bonding interactions, J. Phys. Chem. C 113 (2009) 20666–20673.
[14] W.C. Chen, S.W. Kuo, Ortho-Imide and allyl groups effect on highly thermally stable polybenzoxazine/double-decker-shaped polyhedral silsesquioxane hybrids, Macromolecules 51 (2018) 9602–9612.
[15] K. Zhang, X. Yu, S.W. Kuo, Outstanding dielectric, and thermal properties of main chain-type poly(benzoxazine-co-imide-co-siloxane)-based cross-linked networks, Polym. Chem. 10 (2019) 2387–2396.
[16] M.G. Mohamed, S.W. Kuo, Crown ether–functionalized polybenzoxazine for metal ion Adsorption, Macromolecules 53 (2020) 2420–2429.
[17] B. Akkus, B. Kiskan, Y. Yagci, Combining polybenzoxazines and polybutadienes via simultaneous inverse and direct vulcanization for flexible and recyclable thermosets by polysulfide dynamic bonding, Polym. Chem. 10 (2019) 5743–5750.
[18] A.Q. Dayo, B.C. Gao, J. Wang, W.b. Liu, M. Derradji, A.H. Shah, A.A. Babar, Natural hemp fiber reinforced polybenzoxazine composites: curing behavior, mechanical and thermal properties, Compos. Sci. Technol. 144 (2017) 114–124.
[19] M.G. Mohamed, C.H. Hsiao, K.C. Hsu, F.H. Lu, H.K. Shih, S.W. Kuo, Supramolecular functionalized polybenzoxazines from azobenzene carboxylic acid/azobenzene pyridine complexes: synthesis, surface properties, and specific interactions, RSC Adv. 5 (2015) 12763–12772.
[20] B. Akkus, B. Kiskan, Y. Yagci, Cyanuric chloride as a potent catalyst for the reduction of curing temperature of benzoxazines, Polym. Chem. 11 (2020) 1025–1032.
[21] K. Zhang, L. Han, P. Froimowicz, H. Ishida, A smart latent catalyst containing o-trifluoroacetamide functional benzoxazine: precursor for low temperature formation of very high Performance polybenzoxazole with low dielectric constant and high thermal stability, Macromolecules 50 (2017) 6552–6560.
[22] R.C. Lin, M.G. Mohamed, S.W. Kuo, Benzoxazine/triphenylamine-based dendrimers prepared through facile one-pot Mannich condensations, Macromol. Rapid Commun. 38 (2017) 1700251.
[23] C.S. Liao, C.F. Wang, H.C. Lin, H.Y. Chou, F.C. Chang, Tuning the surface free energy of polybenzoxazine thin films, J. Phys. Chem. C 112 (2008) 16189–16191.

[24] S. Zachariah, Y.L. Liu, Nanocomposites of polybenzoxazine-functionalized multiwalled carbon nanotubes and polybenzoxazine for anticorrosion application, Compos. Sci. Technol. 194 (2020) 108169.
[25] B. Kiskan, G. Demiray, Y. Yagci, Thermally curable polyvinyl chloride via click chemistry, J. Polym. Sci., Part A: Polym. Chem. 46 (2008) 3512–3518.
[26] Z. Deliballi, B. Kiskan, Y. Yagci, Advanced polymers from simple benzoxazines and phenols by ring-opening addition reactions, Macromolecules 53 (2020) 2354–2361.
[27] R.C. Lin, M.G. Mohamed, K.C. Hsu, J.Y. Wu, Y.R. Jheng, S.W. Kuo, Multivalent photo-crosslinkable coumarin-containing polybenzoxazines exhibiting enhanced thermal and hydrophobic surface properties, RSC Adv. 6 (2016) 10683–10696.
[28] C. Ma, L. Han, Z. Ma, H. Ishida, Preparation and characterization of carbon fiber reinforced polybenzoxazine and polybenzoxazole composites from the same precursor: use of a smart, ortho-substituted and amide-co-imide functional matrix, Compos. Sci. Technol. 195 (2020) 108205.
[29] T. Takeichi, T. Kano, T. Agag, Synthesis and thermal cure of high molecular weight polybenzoxazine precursors and the properties of the thermosets, Polymer 46 (2005) 12172–12180.
[30] J. Jang, H. Yang, Toughness improvement of carbon-fibre/polybenzoxazine composites by rubber modification, Compos. Sci. Technol. 60 (2000) 457–463.
[31] R. Ganfoud, L. Puchot, T. Fouquet, P. Verge, H-bonding supramolecular interactions driving the dispersion of kaolin into benzoxazine: a tool for the reinforcement of polybenzoxazines thermal and thermo-mechanical properties, Compos. Sci. Technol. 110 (2015) 1–7.
[32] T. Agag, H. Tsuchiya, T. Takeichi, Novel organic–inorganic hybrids prepared from polybenzoxazine and titania using sol–gel process, Polymer 45 (2004) 7903–7910.
[33] H.K. Shih, C.C. Hsieh, M.G. Mohamed, C.Y. Zhu, S.W. Kuo, Ternary polybenzoxazine/POSS/SWCNT hybrid nanocomposites stabilized through supramolecular interactions, Soft Matter 12 (2016) 1847–1858.
[34] P.C. Ma, N.A. Siddiqui, G. Marom, J.K. Kim, Dispersion and functionalization of carbon nanotubes for polymer-based nanocomposites: a review, Composer Part A Appl. Sci. Manuf. 41 (2010) 1345–1367.
[35] D. Tasis, N. Tagmatarchis, A. Biano, M. Prato, Chemistry of carbon nanotubes, Chem. Rev. 106 (2006) 1105–1136.
[36] Q. Chen, R. Xu, D. Yu, Multiwalled carbon nanotube/polybenzoxazine nanocomposites: preparation, characterization and properties, Polymer 47 (2006) 7711–7719.
[37] C.W. Huang, M.G. Mohamed, C.Y. Zhu, S.W. Kuo, Functional supramolecular polypeptides involving π–π stacking and strong hydrogen-bonding interactions: a conformation study toward carbon nanotubes (CNTs) dispersion, Macromolecules 49 (2016) 5374–5385.
[38] E.T. Thostenson, Z. Ren, T.W. Chou, Advances in the science and technology of carbon nanotubes and their composites: a review, Compos. Sci. Technol. 61 (2001) 1899–1912.
[39] O. Breuer, U. Sundararaj, Big returns from small fibers: a review of polymer/carbon nanotube composites, Polym. Compos. 25 (2004) 630–645.
[40] J.N. Coleman, U. Khan, Y.K. Gun'ko, Mechanical reinforcement of polymers using carbon nanotubes, Adv. Mater. 18 (2006) 689–706.
[41] M. Moniruzzaman, K.I. Winey, Polymer nanocomposites containing carbon nanotubes, Macromolecules 39 (2006) 5194–5205.
[42] R. Andrews, M.C. Weisenberger, Carbon nanotube polymer composites, Curr. Opin. Solid State Mater. Sci. 8 (2004) 31–37.
[43] M.T. Byrne, Y.K. Gun'ko, Recent advances in research on carbon nanotube–polymer composites, Adv. Mater. 22 (2010) 1672–1688.
[44] N.G. Sahoo, S. Rana, J.W. Cho, L. Li, S.H. Chan, Polymer nanocomposites based on functionalized carbon nanotubes, Prog. Polym. Sci. 35 (2010) 837–867.
[45] Z. Spitalsky, D. Tasis, K. Papagelis, C. Galiotis, Carbon nanotube–polymer composites: chemistry, processing, mechanical and electrical properties, Prog. Polym. Sci. 35 (2010) 357–401.
[46] P.S. Goh, A.F. Ismail, B.C. Ng, Directional alignment of carbon nanotubes in polymer matrices: contemporary approaches and future advances, Compos. A: Appl. Sci. Manuf. 56 (2014) 103–126.
[47] S. Iijima, Helical microtubules of graphitic carbon, Nature 354 (1991) 56–58.
[48] E. Thostenson, Z. Ren, T.W. Chou, Advances in the science and technology of carbon nanotubes and their composites: a review, Compos. Sci. Technol. 61 (2001) 1899–1912.
[49] N.G. Sahoo, S. Rana, J.W. Cho, L. Li, S.H. Chan, Polymer nanocomposites based on functionalized carbon nanotubes, Prog. Polym. Sci. 35 (2010) 837–867.
[50] N. Ramdani, J. Wang, H. Wang, T. T Feng, M. Derradji, W.B. Liu, Mechanical and thermal properties of silicon nitride reinforced polybenzoxazine nanocomposites, Compos. Sci. Technol. 105 (2014) 73–79.
[51] M.G. Mohamed, R.C. Lin, S.W. Kuo, in: H. " Ishida, P. Frimowicz (Eds.), "Polybenzoxazine/Carbon Nanotube Composites" in "Advanced and Emerging Polybenzoxazine Science and Technology, Elsevier, Amsterdam, 2017.
[52] L. Sun, X. Wang, Y. Wang, Q. Zhang, Roles of carbon nanotubes in novel energy storage devices, Carbon 122 (2017) 462–474.
[53] B.J. Landi, R.P. Raffaelle, M.J. Heben, J.L. Alleman, W. VanDerveer, T. Gennett, Single wall carbon Nanotube−Nafion composite actuators, Nano Lett. 2 (2002) 1329–1332.
[54] L. Dumas, L. Bonnaud, M. Olivier, P. Dubois, Facile preparation of a novel high performance benzoxazine-CNT based nano-hybrid network exhibiting outstanding thermo-mechanical properties, Chem. Commun. 49 (2013) 9543–9545.
[55] M.G. Mohamed, K.C. Hsu, S.W. Kuo, Bifunctional polybenzoxazine nanocomposites containing photo-crosslinkable coumarin units and pyrene units capable of dispersing single-walled carbon nanotubes, Polym. Chem. 6 (2015) 2423–2433.
[56] G.M. Mohamed, C.H. Hsiao, F. Luo, L. Dai, S.W. Kuo, Multifunctional polybenzoxazine nanocomposites containing photoresponsive azobenzene units, catalytic carboxylic acid groups, and pyrene units capable of dispersing carbon nanotubes, RSC Adv. 5 (2015) 45201–45212.
[57] L. Dumas, L. Bonnaud, M. Olivier, M. Poorteman, P. Dubois, Multiscale benzoxazine composites: the role of pristine CNTs as efficient reinforcing agents for high-performance applications, Compos. B Eng. 112 (2017) 57–65.
[58] J. Li, K. Shi, M. Drechsler, B.Z. Tang, J. Huang, Y. Yan, A supramolecular fluorescent vesicle based on a coordinating aggregation induced emission amphiphile: insight into the role of electrical charge in cancer cell division, Chem. Commun. 52 (2016) 12466–12469.
[59] J.B. Xiong, Y.X. Yuan, L. Wang, J.P. Sun, W.G. Qiao, H.C. Zhang, M. Duan, H. Han, S. Zhang, Y.S. Zheng, Evidence for aggregation-induced emission from free rotation restriction of double bond at excited state, Org. Lett. 20 (2018) 373–376.
[60] X. Zhang, M.G. Mohamed, Z. Xin, S.W. Kuo, A tetraphenylethylene-functionalized benzoxazine and Copper(II) acetylacetonate form a high-performance polybenzoxazine, Polymer 201 (2020) 122552.
[61] C.C. Yang, Y.C. Lin, P.I. Wang, D.J. Liaw, S.W. Kuo, Polybenzoxazine/single-walled carbon nanotube nanocomposites stabilized through noncovalent bonding interactions, Polymer 55 (2014) 2044–2050.
[62] M.G. Mohamed, M.Y. Tsai, W.C. Su, A.F.M. EL-Mahdy, C.F. Wang, C.F. Huang, L. Dai, T. Chen, S.W. Kuo, Nitrogen-Doped microporous carbons derived from azobenzene and nitrile-functionalized polybenzoxazines for $CO_2$ uptake, Mater. Today Commun. 24 (2020) 101111.
[63] K. Zhang, X. Yu, Catalyst-free and low-temperature Terpolymerization in a single-component benzoxazine resin containing both norbornene and acetylene functionalities, Macromolecules 51 (2018) 6524–6533.
[64] J.Y. Wu, M.G. Mohamed, S.W. Kuo, Directly synthesized nitrogen-doped microporous carbons from polybenzoxazine resins for carbon dioxide capture, Polym. Chem. 8 (2017) 5481–5489.
[65] H.M. Qi, G.Y. Pan, Y.Q. Zhuang, F.R. Huang, L. Du, Synthesis and characterization of acetylene-terminated polybenzoxazines based on polyaralkyl-phenolic prepolymer, Polym. Eng. Sci. 50 (2010) 1751–1757.
[66] Y. Li, C.Y. Zhang, S.X. Zheng, Microphase separation in polybenzoxazine thermosets containing benzoxazine-terminated poly(ethylene oxide) telechelics, Eur. Polym. J. 47 (2011) 1550–1562.
[67] H. Wang, J. Wang, X. He, T. Feng, N. Ramdani, M. Luan, W. Liu, X. Xu, Synthesis of novel furan-containing tetrafunctional fluorene-based benzoxazine monomer and its high-performance thermoset, RSC Adv. 4 (2014) 64798–64801.
[68] Y.P. Chen, X.Y. He, A.Q. Dayoa, J.Y. Wang, W. Liu, J. Wang, T. Tang, Synthesis and characterization of cardanol containing tetra-functional fluorene-based benzoxazine resin having two different oxazine ring structures, Polymer 179 (2019) 121620–121626.
[69] H.E. Kissinger, Reaction kinetics in differential thermal analysis, Anal. Chem. 29 (1957) 1702–1706.
[70] M. Chapartegui, J. Barcena, X. Irastorza, C. Elizetxea, M. Fernandez, A. Santamaria, Analysis of the conditions to manufacture a MWCNT Bucky paper/benzoxazine nanocomposite, Compos. Sci. Technol. 72 (2012) 489–497.
[71] M. Kaleemullah, S.W. Khan, J.K. Kim, Effect of surfactant treatment on thermal stability and mechanical properties of CNT/polybenzoxazine nanocomposites, Compos. Sci. Technol. 72 (2012) 1968–1976.
[72] C. Zúñiga, L. Bonnaud, G. Lligadas, J.C. Ronda, M. Galià, V. Cádiz, P. Dubois, Convenient and solventless preparation of pure carbon nanotube/polybenzoxazine nanocomposites with low percolation threshold and improved thermal and fire properties, J. Mater. Chem. 2 (2014) 6814–6822.
[73] Y. Li, S. Zheng, X. Liu, P. Li, L. Sun, R. Yang, S. Wang, Z. Wu, X. Bao, W.Q. Deng, Conductive microporous covalent triazine-based framework for high-performance electrochemical capacitive energy storage, Angew. Chem. Int. Ed. 57 (2018) 7992–7996.
[74] Y. Liu, X. Hao, L. Wang, Y. Xu, J. Liu, X. Tian, B. Yao, Facile synthesis of porous carbon materials with extra high nitrogen content for supercapacitor electrodes, New J. Chem. 43 (2019) 3713–3718.
[75] M.G. Mohamed, A.F.M. EL-Mahdy, M.M.M. Ahmed, S.W. Kuo, Direct synthesis of microporous bicarbazole-based covalent triazine frameworks for high-performance energy storage and carbon dioxide uptake, ChemPlusChem 84 (2019) 1767–1774.